

## SUPPORTING INFORMATION

### **Impact of functionalized linkers in the energy landscape of ZIFs**

**Raimondas Galvelis,<sup>a</sup> Ben Slater,<sup>a</sup> Robin Chaudret,<sup>b</sup> Benoit Creton,<sup>b</sup> Carlos Nieto-Dragi,<sup>b</sup>  
Caroline Mellot-Draznieks<sup>a,c</sup>**

<sup>a</sup> Department of Chemistry, University College London, 20 Gordon St., London, WC1H 0AJ, UK

<sup>b</sup> IFP Energies nouvelles, 1-4 avenue de Bois-Préau, 92852 Rueil-Malmaison, France

<sup>c</sup> Laboratoire de Chimie des Processus Biologiques, Collège de France-CNRS FRE3488, 11 place  
Marcelin-Berthelot, 75005 Paris, France

## I- DFT-D3 calculations

Electronic energy was minimized with the orbital transformation (OT)<sup>i</sup> method. The convergence criterion for the self-consistent field (SCF) procedure was set to  $1.0 \times 10^{-7}$ . The nuclear and core electronic densities were modelled with the relativistic, norm-conserving, separable, dual-space Gaussian-type pseudo-potentials of Goedecker-Teter-Hutter (GTH)<sup>ii,iii</sup> and the valence electronic density represented by the hybrid Gaussian-type and plane-wave (GPW)<sup>iv</sup> basis sets scheme. All atoms had molecular optimised DZVP<sup>v</sup> basis sets. In our previous work, the basis sets has been validated with a plane-wave code to have a small basis set super-position error (BSSE). The plane wave cut-off was set to 400 Ry. Periodic boundary conditions and the  $\Gamma$ -point only sampling of k-space was used (the minimum simulation cell length was 10.3 Å). Structure optimisations were done using Broyden–Fletcher–Goldfarb–Shanno (BFGS) optimizer with simultaneous relaxation of simulation cell parameters, and atomic positions. No symmetry constrains (*P1* space group) was imposed. Each structure was considered relaxed then maximum force, RMS force, maximum displacement, RMS displacement were below  $4.5 \times 10^{-4}$  a.u.,  $3.0 \times 10^{-4}$  a.u.,  $3.0 \times 10^{-3}$  a.u.,  $1.5 \times 10^{-3}$  a.u., respectively, and pressure deviation smaller than 0.01 GPa.

**Topological Energy.** Seven Li-L-BH<sub>3</sub> clusters (one for each linker L) were constructed in order to mimic the environment of each linker in a ZIF and preserve its charge neutrality. The structure of Li—(2-MeIm)—BH<sub>3</sub> model is illustrated in figure S1. In order to mimic the range of framework densities in BIFs, three Li-L-BH<sub>3</sub> clusters were constructed for each type of ligand, fixing the Li and B atoms at 5.4, 5.6 and 5.8 Å (a typical range of Li-B distances in BIFs). The remaining atoms of the clusters were relaxed with the same DFT set-up as used for ZIFs relaxation, with the exception of periodic boundary conditions. The total electronic energies of the relaxed clusters,  $E^{(d)}_L$ , are given in Table S1, where  $d$  is the fixed distance between Li and B atoms. It is apparent that the total electronic energy,  $E^{(d)}_L$ , is quite insensitive to the distance between Li and B atoms, indicating quite shallow inter-atomic potential between Li—N, since B—N bond is known to be much stronger. This means that  $\Delta E_{T-L}$  term could be assumed to be constant and negligible. The possible error,  $\varepsilon_L$ , of the approximation is estimated in (4) and given Table S1.

$$\varepsilon_L = \max \Delta E_L^{(d)} - \min \Delta E_L^{(d)} \quad (1)$$

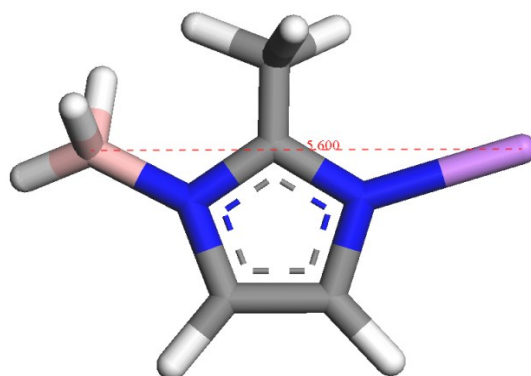


**Figure S1.** The structure of Li-(2MeIm)-BH<sub>3</sub> model (Li – violet, B – pink, O – red, C – grey, and H – white).

**Table S1.** The DFT-D energies of model clusters.

	Im	2-MeIm	4-MeIm	5-MeIm	2,4-MeIm	2,5-Me <sub>2</sub> Im	4,5-Me <sub>2</sub> Im
d, Å	$E^{(d)}_L$ , kJ/mol						
5.4	-133370.836	-151463.560	-151456.258	-151460.167	-169548.708	-169549.112	-169545.339
5.6	-133371.447	-151463.433	-151457.137	-151460.515	-169548.802	-169549.318	-169545.977
5.8	-133363.701	-151454.522	-151449.790	-151451.917	-169540.664	-169540.597	-169538.022
d, Å	$\Delta E^{(d)}_L$ , kJ/mol						
5.4	0.0	-18092.724	-18085.421	-18089.330	-36177.871	-36178.276	-36174.503
5.6	0.0	-18091.987	-18085.691	-18089.069	-36177.355	-36177.872	-36174.531
5.8	0.0	-18090.821	-18086.089	-18088.215	-36176.962	-36176.896	-36174.321
$\Delta E_L$ , kJ/mol	0.0	-18091.844	-18085.734	-18088.871	-36177.396	-36177.681	-36174.451
$\epsilon_L$ , kJ/mol	0.0	1.903	0.668	1.115	0.909	1.380	0.210

**Table S2.** The comparison of experimental (*italic*) and simulated (*straight*) structures parameters of LiB ZIFs. The relative errors are given in parantheses (%). BIF-9 and BIF-2 framework contains guest molecules resulting in a poor agreement between simulated and experimental data.

	BIF-1	BIF-2*	BIF-3	BIF-9*	BIF-11
Topology	zni	dia	SOD	RHO	SOD
Linker	Im	2-MeIm	2-MeIm	4-MeIm	2,4-MeIm
Space group	<i>I4<sub>1</sub>cd</i>	<i>I-4</i>	<i>P-43n</i>	<i>P432</i>	<i>P-43n</i>
	<i>I4<sub>1</sub>cd</i>	<i>I-4</i>	<i>P-43n</i>	<i>P432</i>	<i>P-43n</i>
a, Å	22.349	7.238	15.957	27.590	16.428
	<i>22.504</i>	<i>7.582</i>	<i>16.031</i>	<i>26.292</i>	<i>16.314</i>
	(-0.69)	(-4.54)	(-0.46)	(4.94)	(0.70)
b, Å	22.352	7.238	15.957	27.590	16.428
	<i>22.504</i>	<i>7.582</i>	<i>16.031</i>	<i>26.292</i>	<i>16.314</i>
	(-0.67)	(-4.54)	(-0.46)	(4.94)	(0.70)
c, Å	11.474	16.670	15.957	27.590	16.428
	<i>11.515</i>	<i>16.428</i>	<i>16.031</i>	<i>26.292</i>	<i>16.314</i>
	(-0.36)	(1.47)	(-0.46)	(4.94)	(0.70)
Volume, Å <sup>3</sup>	5731.81	873.21	4063.04	21001.74	4433.90
	<i>5831.40</i>	<i>944.34</i>	<i>4119.93</i>	<i>18174.90</i>	<i>4341.76</i>
	(-1.71)	(-7.53)	(-1.38)	(15.55)	(2.12)

\* Experimental structure contains guest molecules.

\*\* The non-zeolitic topologies (*dia* and *zni*), which are known as LiB-based and Zn-based ZIFs, were not included in the present work in methyl-substituted versions. They possess low densities and, mainly, exist with unsubstituted imidazolate linkers. The incorporation of bulkier linker to low density frameworks might thus be complicated since steric hindrances might prevent internal relaxation giving bias results on the initial structures.

## Geometrical features in methyl-substituted BIFs.

We have carefully analyzed the variation of structural parameters among all studied ZIFs in terms of distances, angles and torsions. We assume that ZIFs are made of relatively rigid organic imidazole linkers connected to  $\text{Li}^+$  and  $\text{B}^{3+}$  cations via relatively softer bonds. For this purpose we evaluated the variation of three atomic distances, Li-B, Li-N and B-N (Figure S2), three angles, N-Li-N, N-B-N and Li-Im-B (Figure S3), where Im is the geometrical centre of the imidazolate ring) and two torsions, Li-N-C-N and LI-N-C-N (Figure S5). Li-N and B-N distances characterize the strength of the corresponding bonds, and N-Li-N and N-B-N angles characterize the rigidity of the  $[\text{LiN}_4]$  and  $[\text{BN}_4]$  tetrahedra, respectively. Systematic trends between the topological density and geometrical features are not directly apparent. Nevertheless, we observe a number of recurrent features: (i) comparing the Li-N and B-N distances, there is a much larger variability of the former in the different frameworks, in line with the stronger and less compliant B-N bonds. In turn, the larger the statistical distribution of B-N distances around an equilibrium distance of 1.54-1.56 Å (or the larger the statistical distribution of Li-B distances), the less stable the corresponding structures. Typically, simulated structures possessing B-N distances in the 1.57 Å -1.58 Å range are clearly identified as unstable ones. This is particularly visible among LiB-ZIFs simulated with 2,4-MeIm and 2,5-MeIm. (ii) a comparison of N-Li-N and N-B-N angles reveals that the  $[\text{BN}_4]$  tetrahedral are more geometrically constrained than the  $[\text{LiN}_4]$  ones. As a result, structures combining a large statistical distribution of B-N distances and distorted  $[\text{BN}_4]$  tetrahedral exhibit among the largest topological energies i.e. the less stable structures. The Li-Im-B angles are very flexible, covering among the most stable structures a rather large range (133°-145°), which is in contrast with the restricted angle observed in their zeolitic inorganic counterpart

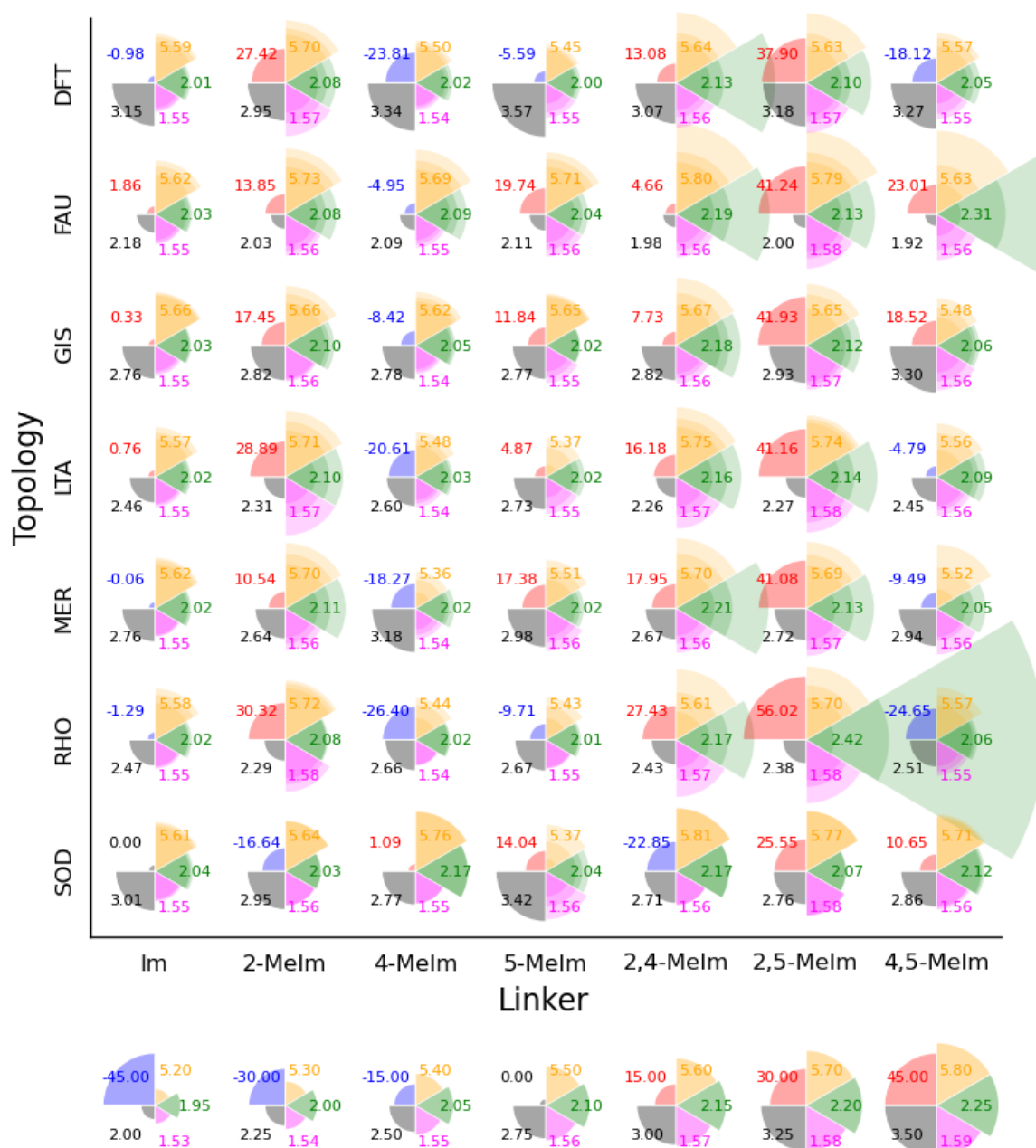


**Figure S2.** Bubble plot of Li-B distance (yellow), Li-N distance (green) and B-N distance (magenta), density (grey) and energy (blue/red) in lithium-boron-based ZIFs. The three concentric segments of angle ( $\text{\AA}$ ) disks represent minimum, mean and maximum values, respectively.

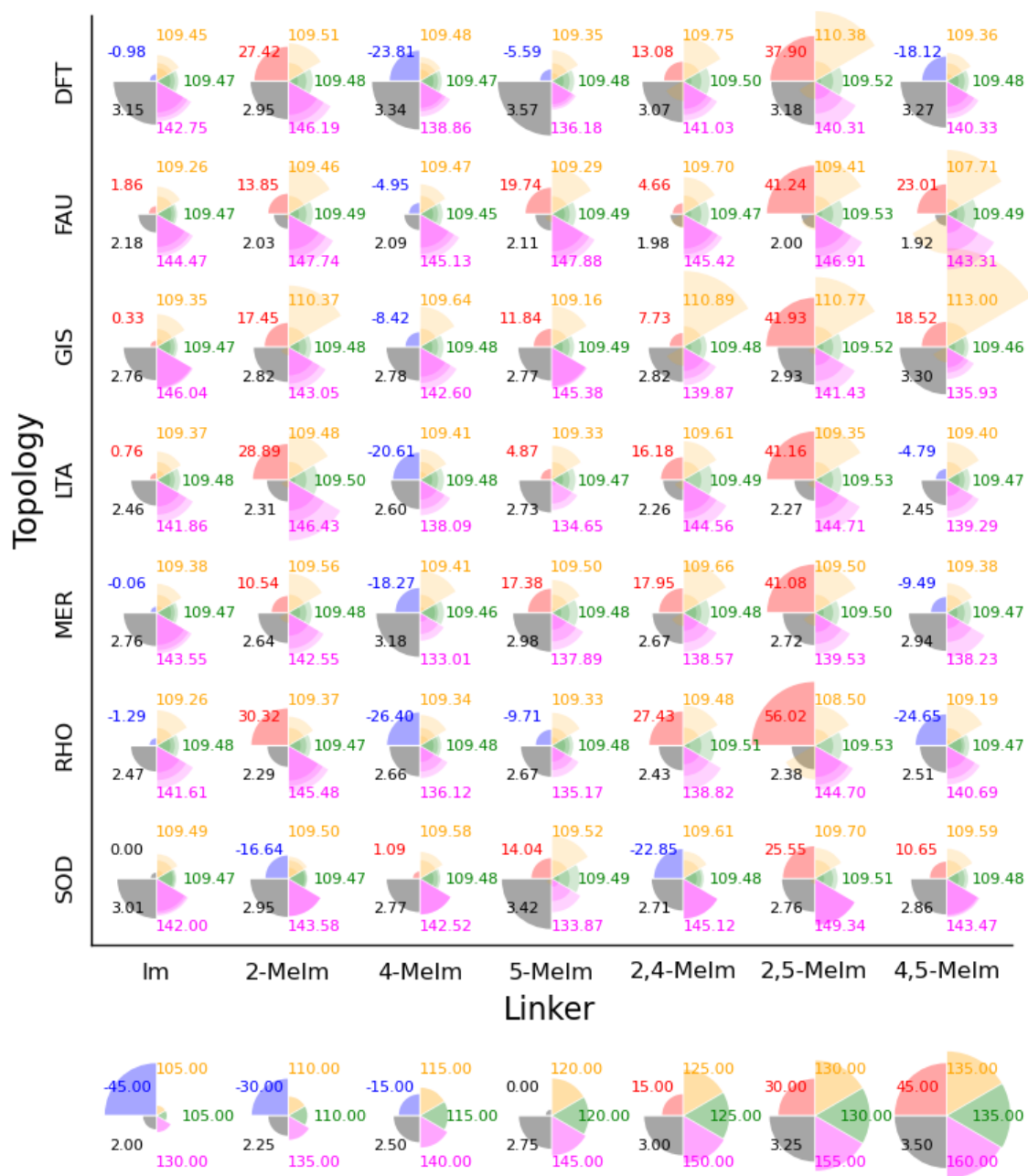


**Figure S3.** Bubble plot of N-Li-N angle (yellow), N-B-N angle (green), and Li-Im-B angle (magenta), energy (blue and red), density (grey) for LiB-based ZIFs. Li-Im-B is the angle between Li, the geometrical centre of imidazolate ring (Im), and B. The three concentric segments of angle ( $^{\circ}$ ) disks represent minimum, mean, and maximum values, respectively.

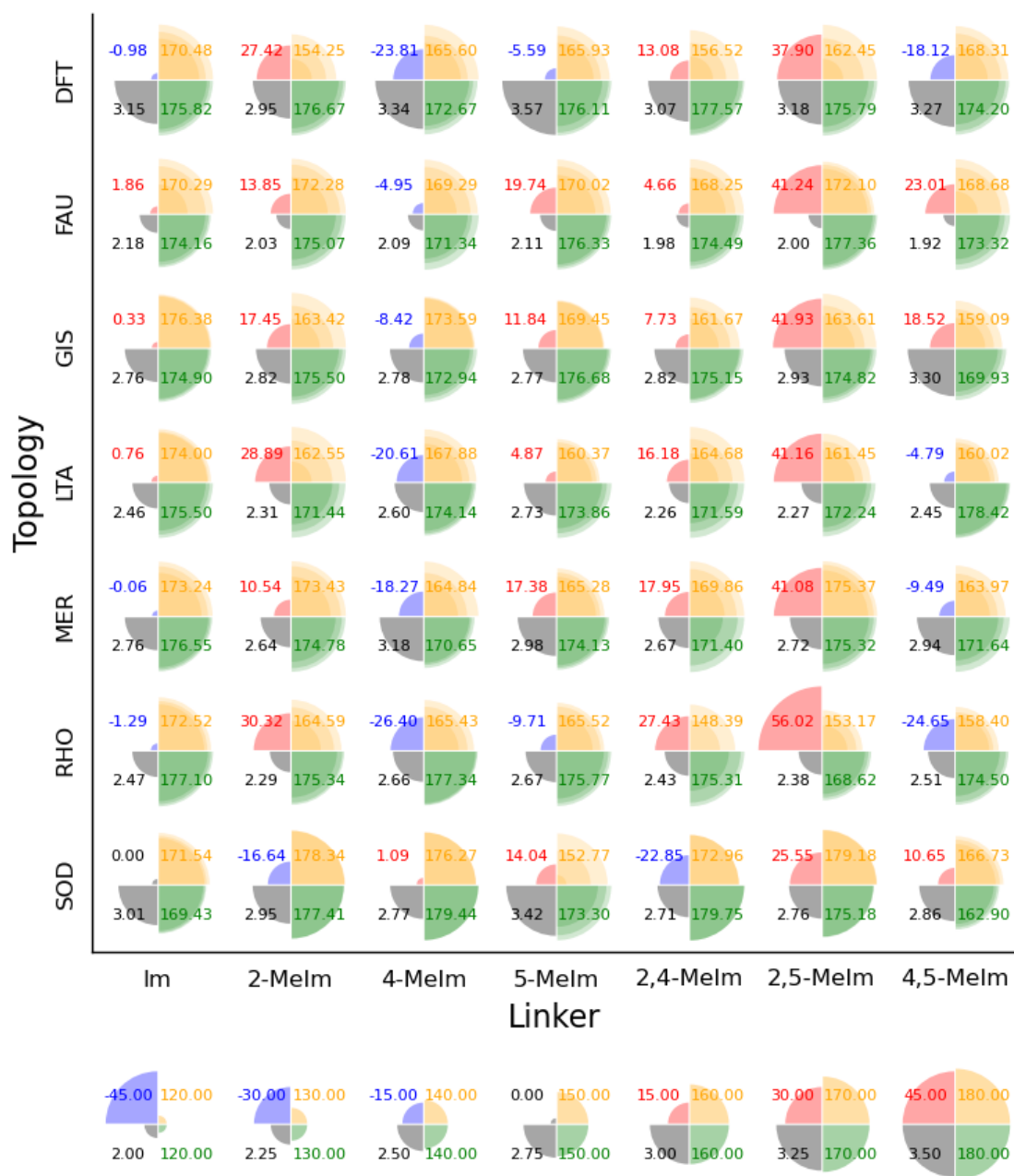


**Figure S4.** Bubble plot of Li-N-C-N torsion angle (yellow), and B-N-C-N torsion angle (green), energy (blue/red) and density (grey) for LiB-based ZIFs. Li-N-C-N and B-N-C-N are torsion angles between Li-N and B-N bonds, respectively, and the effectively the plane of imidazole ring. The three concentric segments of torsion angle ( $^{\circ}$ ) disks represent minimum, mean, and maximum values, respectively.

## II- QSPR calculations

**Table S3.** Database used for the development of the QSPR model presented in equation (8). Parameters values for equation (8) are regressed only on data points belonging to the Training set.

Topology	Linker	Set	$\Delta E_T$ (kJ/mol)	Topology	Linker	Set	$\Delta E_T$ (kJ/mol)
DFT	5-Melm	Training	-5.592	MER	5-Melm	Training	17.379
DFT	4-Melm	Training	-23.811	MER	4,5-Melm	Training	-9.488
DFT	4,5-Melm	Training	-18.119	MER	2-Melm	Training	10.537
DFT	2-Melm	Training	27.423	MER	2,5-Melm	Training	41.08
DFT	2,5-Melm	Training	37.903	MER	2,4-Melm	Training	17.951
DFT	2,4-Melm	Training	13.084	RHO	Im	Training	-1.293
FAU	Im	Training	1.859	RHO	5-Melm	Training	-9.712
FAU	5-Melm	Training	19.74	RHO	4-Melm	Training	-26.399
FAU	4-Melm	Training	-4.946	RHO	2-Melm	Training	30.324
FAU	4,5-Melm	Training	23.006	RHO	2,5-Melm	Training	56.017
FAU	2-Melm	Training	13.846	RHO	2,4-Melm	Training	27.431
FAU	2,5-Melm	Training	41.24	SOD	Im	Training	0
GIS	Im	Training	0.331	SOD	4-Melm	Training	1.092
GIS	5-Melm	Training	11.836	SOD	4,5-Melm	Training	10.647
GIS	4-Melm	Training	-8.416	SOD	2-Melm	Training	-16.644
GIS	4,5-Melm	Training	18.518	SOD	2,5-Melm	Training	25.552
GIS	2,5-Melm	Training	41.932	SOD	2,4-Melm	Training	-22.852
GIS	2,4-Melm	Training	7.726	DFT	Im	Validation	-0.976
LTA	Im	Training	0.759	FAU	2,4-Melm	Validation	4.663
LTA	5-Melm	Training	4.866	GIS	2-Melm	Validation	17.448
LTA	4-Melm	Training	-20.608	LTA	2,5-Melm	Validation	41.162
LTA	4,5-Melm	Training	-4.791	MER	4-Melm	Validation	-18.267
LTA	2-Melm	Training	28.89	RHO	4,5-Melm	Validation	-24.651
LTA	2,4-Melm	Training	16.175	SOD	5-Melm	Validation	14.043
MER	Im	Training	-0.063				

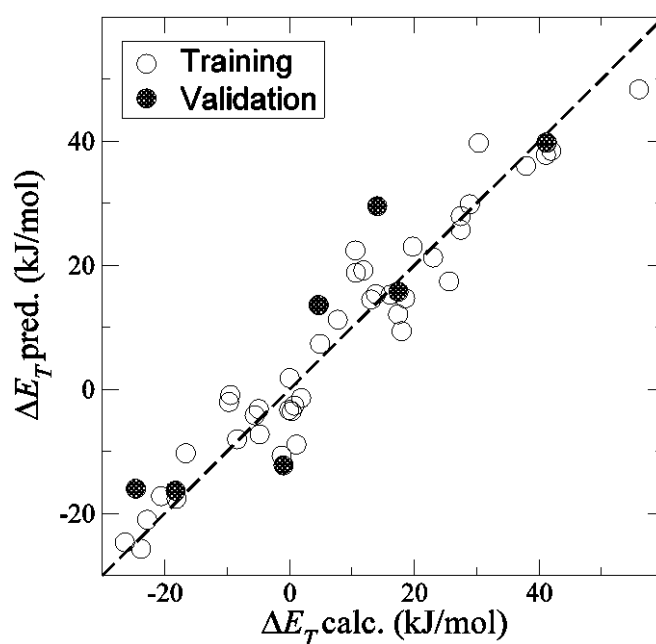


**Figure S5.** Plot of predicted relative topological energies with equation (8) versus relative topological energies calculated by DFT-D.

**Table S4.** Parameter values for equation (8).  $R^2$  is the coefficient of determination, RMSD is the root mean square deviation, and AAD is the average absolute deviation.

Topology	DFT	FAU	GIS	LTA	MER	RHO	SOD
<i>FD</i>	17.7	13.3	16.4	14.2	16.4	14.5	16.7
Topology	DFT	FAU	GIS	LTA	MER	RHO	SOD
$\beta'$	15.000	-8.451	-5.933	7.262	0.526	25.197	-37.328
$\gamma'$	-5.114	6.550	3.798	-6.260	-4.682	-5.680	-2.399
$\delta'$	-8.829	7.494	5.793	-6.953	-1.493	-8.278	10.785
$\varepsilon'$	-1.456	-1.592	4.042	-0.570	4.230	-7.865	10.144
$\alpha$	-2.502						
$\beta$	25.195						
$\gamma$	-8.319						
$\delta$	16.915						
$\varepsilon$	33.457						
	Training	Validation					
$R^2$	0.933	0.824					
RMSD	5.1	8.7					
AAD	4.1	7.0					

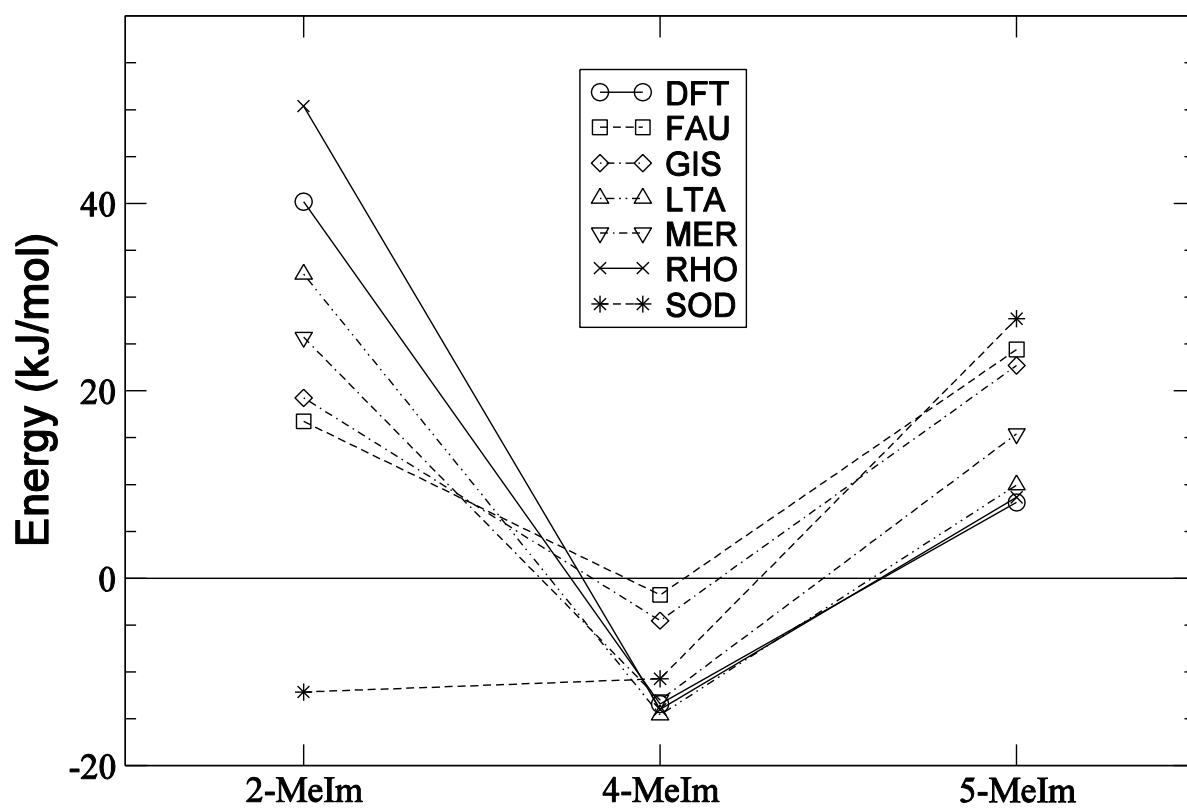


**Figure S6.** Energetic contribution in equation (8) when placing a methyl group on the imidazole linker on positions 2, 4, or 5 for all zeotypes considered in this study.

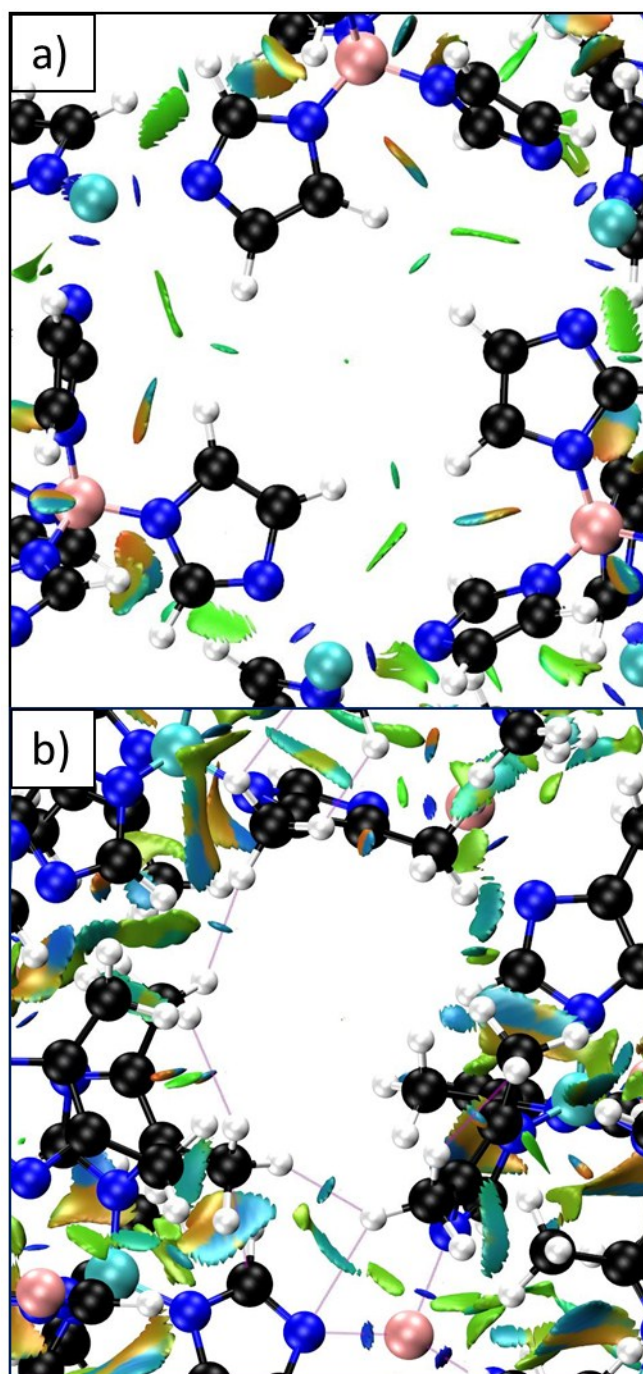


**Figure S7.** NCI analysis of **SOD-Im** (a) and of the **SOD-4,5-Me<sub>2</sub>Im-** (b) topologies centred on a 6-ring window.

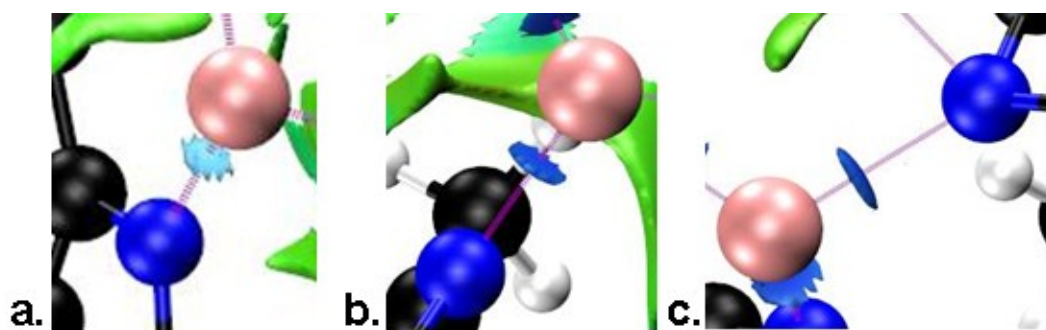


**Figure S8.** NCI analysis of the Li-Im interactions in the **SOD-2,4-Me<sub>2</sub>Im** (a), **SOD-2-MeIm** (b) and **SOD-4-MeIm** (c) topologies.

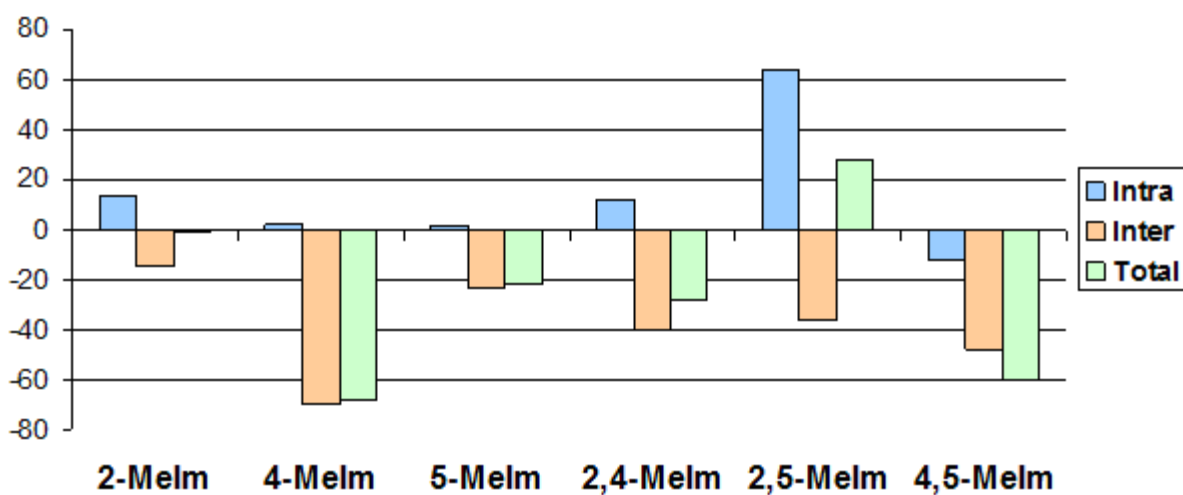


**Figure S9.** Integrated inter, intra and total NCI non-bonded interactions for **SOD** topologies with 2-MeIm, 4-MeIm, 5-MeIm, 2,4-Me<sub>2</sub>Im, 2,5-Me<sub>2</sub>Im, 4,5-Me<sub>2</sub>Im linkers.

<sup>i</sup> VandeVondele, J.; Hutter, J. *J. Chem. Phys.* **2003**, *118*, 4365.

<sup>ii</sup> Goedecker, S. Teter, M.; Hutter, J. *Phys. Rev. B* **1996**, *54*, 1703.

<sup>iii</sup> Krack, M. *Theoretical Chemistry Accounts: Theory, Computation, and Modeling (Theoretica Chimica Acta)* **2005**, *114*, 145-152.

<sup>iv</sup> Lippert G. Hutter J.; Parrinello M. *Molecular Physics* **1997**, *92*, 477-488.

<sup>v</sup> VandeVondele, J.; Hutter, J. *J. Chem. Phys.* **2007**, *127*, 114105.